Microsyst Technol (2005) 11: 1276–1286
DOI 10.1007/s00542-005-0594-5

TECHNICAL PAPER

Xinghui Huang · Roberto Horowitz · Yunfeng Li

Track-following control with active vibration damping and compensation of a dual-stage servo system

Received: 28 September 2004 / Accepted: 4 January 2005 / Published online: 5 October 2005

Abstract This paper proposes a vibration control scheme for an actuated-slider dual-stage servo system. The control scheme consists of three components: a basic track-following servo loop, a feedback vibration damping loop around the main actuator, the voice coil motor (VCM), and a feedforward vibration compensation loop around the secondary microactuator (MA). A strain gauge sensor fabricated on the surface of the suspension detects airflow-excited structural vibrations and its output is fed to the feedback damping and feedforward compensation loops simultaneously. A higher sampling rate can be utilized for both the feedback damping and feedforward compensation controllers to achieve better performance. Simulation results show that the track-misregistration (TMR) resulting from the airflow-excited structural vibrations can be greatly attenuated, achieving a total reduction in TMR by 27% over the conventional dual-stage actuation without dedicated vibration control. Based on this control scheme and simulation results, projection of the system performance to the target of 500k tracks per inch (TPI) is performed, yielding some guidelines on how to improve disk drive's operational conditions and control effect in order to approach the targeted areal density, 3σ TMR budget of 5 nm.

1 Introduction

With the technological advances and breakthroughs in computer hard disk drives (HDDs), there has been a continuing trend of increasing the areal storage density from 100 Mb/in^2 in 1991 to 100 Gb/in^2, which was achieved recently (Seagate 2003), and towards the goal of 1 Tb/in^2 set by the information storage industry. It is predicted that future areal storage density increases will be achieved mainly through an increase in track densities. For an areal density of 1 Tb/in^2, the corresponding track density is about 500k TPI, which implies a track pitch of 50 nm and an allowable 3σ TMR of 5 nm.

To achieve this goal, the closed-loop servo bandwidth has to be increased accordingly for fast settling and effective track following. Dual-stage servo systems have thus been proposed to extend the servo bandwidth. However, it is also expected that with the extended servo bandwidth and increased disk revolution speeds, airflow-excited suspension structural vibrations will become a significant obstacle to achieving even higher track densities. The resonance modes of a suspension usually lie in a frequency range beyond the achievable servo bandwidth, which is mainly limited by the PES sampling rate and computational delay. Thus, TMR due to suspension vibration cannot be sufficiently attenuated with only PES feedback control. On the contrary, with the increased servo bandwidth and further attenuation in the low-frequency range, airflow-excited structural vibrations may be amplified according to Bode's integral theorem (Bode 1945).

There exist several techniques for dealing with the suspension's structural vibrations. A commonly used one is to insert notch filters into the control loop to ensure the stability of servo systems. However, notch filters generally reduce the phase margin and affect the system robustness (Huang et al. 2001). Besides, notch filters can only prevent the control input from exciting those vibration modes but cannot actively compensate for those vibrations excited by airflow disturbances.

The idea of utilizing additional sensors to further increase the servo bandwidth has been explored by several researchers (Pannu and Horowitz 1999; Oboe 2000; Li and Horowitz 2001a; Li et al. 2003). In (Pannu and Horowitz 1999; Oboe 2000), it was proposed to

X. Huang (✉) · R. Horowitz · Y. Li
Department of Mechanical Engineering,
University of California at Berkeley,
Berkeley, CA 94720, USA
E-mail: xhhuang@me.berkeley.edu

Y. Li
Maxtor Corporation, 500 McCarthy Blvd,
Milpitas, CA 95035, USA

attach an acceleration sensor at a proper location in the HDD to provide a vibration signal for feedforward control. This configuration was based on the single actuator, the VCM. Thus the servo bandwidth cannot be significantly extended due to its single-stage property. In Li et al. (2003), active vibration damping of a dual-stage servo system with a PZT-actuated suspension was proposed and experimentally tested. The main disadvantage of this configuration is that the PZT actuators are located between the E-block arm and the suspension, and thus may still excite the structural resonance modes, which may limit its achievable bandwidth. Moreover, the resonance frequencies of a PZT-actuated suspension are generally lower than a conventional suspension and, as a consequence, are more susceptible to airflow disturbances. For the actuated slider approach, active feedforward vibration compensation has been proposed (Li and Horowitz 2001a). Feedforward control is very effective in cancelling certain disturbances that can either be determined a priori or be measured in real time. One advantage of feedforward control is that there is no stability issue and the performance of feedforward control is also not constrained by Bode's integral identity. Both of the above two approaches need to utilize additional vibration sensors for vibration detection. The vibration signal can be sampled at a higher rate than the PES servo loop in order to achieve a higher bandwidth and hence a better performance.

In this paper, a feedback plus feedforward control scheme is proposed for attenuating airflow-excited suspension vibrations. The control scheme is based on an actuated slider dual-stage servo system, which utilizes a MEMS MA sandwiched between the gimbal and the slider. Vibration control is implemented by a feedback damping controller around the VCM and a feedforward compensator around the MA. Notch filters are not used in the track-following loop since those vibration modes are already adequately suppressed through VCM damping. This paper is organized as follows. Section 2 discusses the system structure and modelling of the actuators and strain sensor. The detailed design procedure and derivation of the proposed vibration control scheme are presented in Sect. 3. Simulation results are shown in Sect. 4. Section 5 performs the TMR projection based on the obtained results. Section 6 concludes this paper.

2 System structure and modelling

Figure 1 illustrates the proposed experimental system configuration. It consists of two actuators: a VCM and an MA located between the suspension tip and the slider. The MA is fabricated using MEMS techniques and can generate rotational motion of the slider relative to the suspension through electrostatic force. Figure 2 shows the MA assembled with a suspension and slider. The feedback loop in the lower part of the figure depicts the basic track-following servo loop, which utilizes only the PES measured by a laser doppler vibrometer (LDV).[1] Strain sensors are fabricated on the surface of the suspension for detecting structural vibrations. The detected vibration signal is fed back to the VCM and fed forward to the MA simultaneously for vibration attenuation.

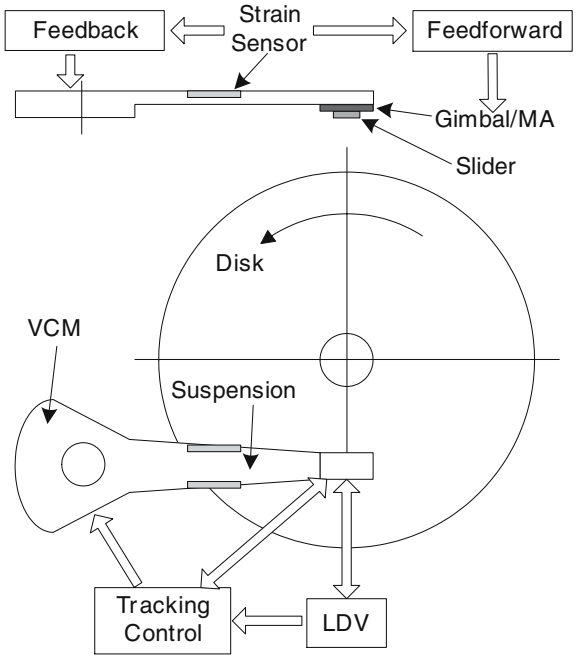

Fig. 1 Dual-stage drive structure and suspension vibration measurement setup

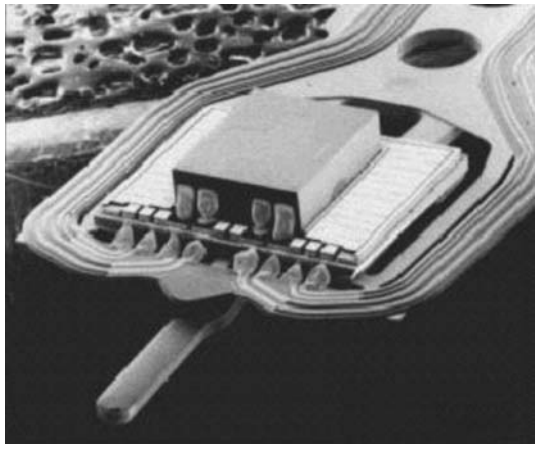

Fig. 2 Photograph of an MA assembled with a suspension and slider (Courtesy of Hitachi Global Storage Technologies)

[1] In actual disk drives, the PES is obtained by subtracting the actual position value read by the magnetic head from the desired position value, not from an LDV.

2.1 VCM assembly dynamics

The suspension model used in this simulation study is based on a newly redesigned suspension from an original one that had been used in our previous simulation and experimental study (Li et al. 2003). The frequency response of the redesigned suspension is shown in Fig. 3. The objective of redesign is to make the suspension stiffer in the transversal direction of data tracks and shift the resonance modes to a higher frequency range, so that less suspension structural vibration will excited by airflow disturbance. This property is desirable in future HDDs where airflow disturbances will become an important obstacle to achieving ultra high track densities.

Strain gauge sensors are fabricated on the surface of the suspension for active vibration control. With strain sensors integrated, the suspension assembly is often referred to as an instrumented suspension. By proper design in sensor locations and orientations, these sensors are sensitive to those modes that can generate off-track motion at the read/write head (off-track modes), while rejecting other irrelevant modes that do not contribute to the head's off-track motion (non-off-track modes). Therefore, the sensor output consists of a combination of those off-track modes constituting the actual head position output but with a possibly different set of coefficients. The transfer functions from the VCM current input to the head position output and to the strain sensor output can be modelled using the following expression:

$$G_V(s) = \frac{A_0}{s^2} + \sum_{i=1}^{N} \frac{A_i}{s^2 + 2\varsigma_i w_i s + w_i^2}, \quad (1)$$

where A_0 is the gain of the rigid body mode, N is the total number of vibration modes being considered, ω_i, ζ_i and A_i are the natural frequency, damping ratio and modal constant of mode i, respectively. These modal parameters can be identified from the measured frequency responses using modal testing techniques. In this simulation study, three resonance modes of the suspension are included. They are located at 7.4 kHz, 10.7 kHz and 13.0 kHz, all with a damping ratio of 0.015.

2.2 Airflow-excited suspension vibration

As mentioned before, the resonance modes of the VCM-suspension assembly may be excited by airflow disturbances around it. Some of these modes are contributive to the head off-track motion, some are not. Figure 4 shows an example of experimental measurements of the head off-track motion and the PZT sensor output from a 3.5″ disk with 7,200 RPM. From the figure, we can see that three major off-track modes, M1, M2 and M3, are excited by airflow disturbances and are also sensed by the strain sensor. In the meantime, the sensor also picks up some non-off-track modes: M4, M5 and M6. These modes are probably the suspension's bending modes excited by airflow disturbances in the out-of-plane direction. Those non-off-track modes need to be filtered out from the sensor measurement in order to implement off-track motion control. In this study, three non-off-track modes are also included in the strain sensor model to investigate their impacts on the system performance.

2.3 Microactuator dynamics

The MA model is derived from the experimental results of a prototype MEMS MA fabricated in our research group. Its frequency response is measured and identified

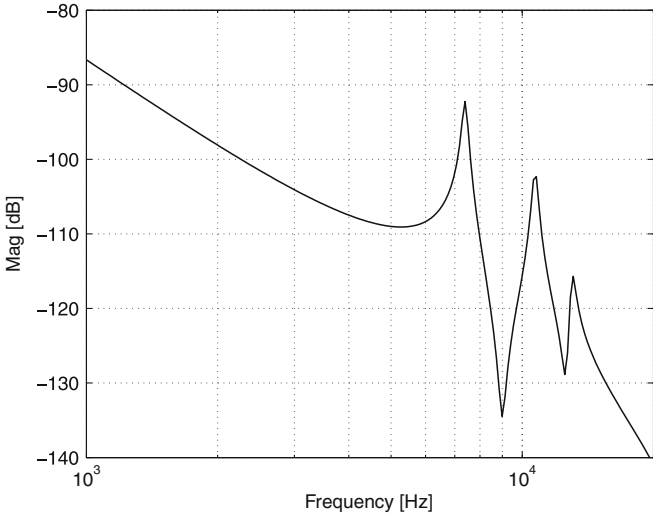

Fig. 3 Magnitude-frequency responses of original and redesigned suspensions

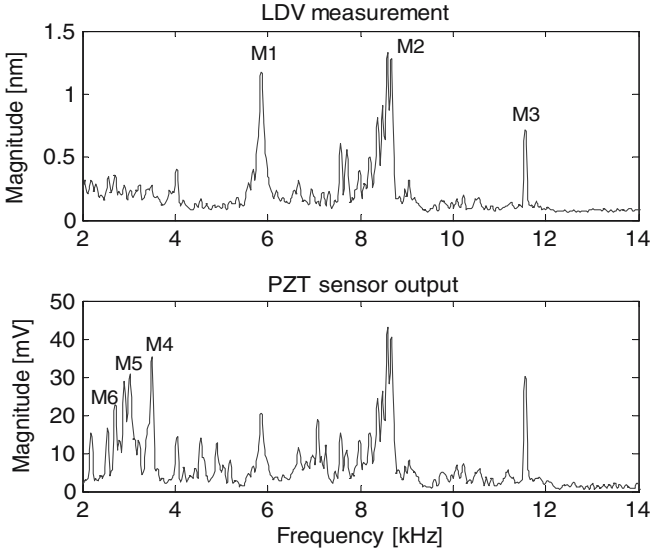

Fig. 4 Frequency spectra of the head off-track motion and the PZT sensor output due to airflow-excited vibrations (Experimental)

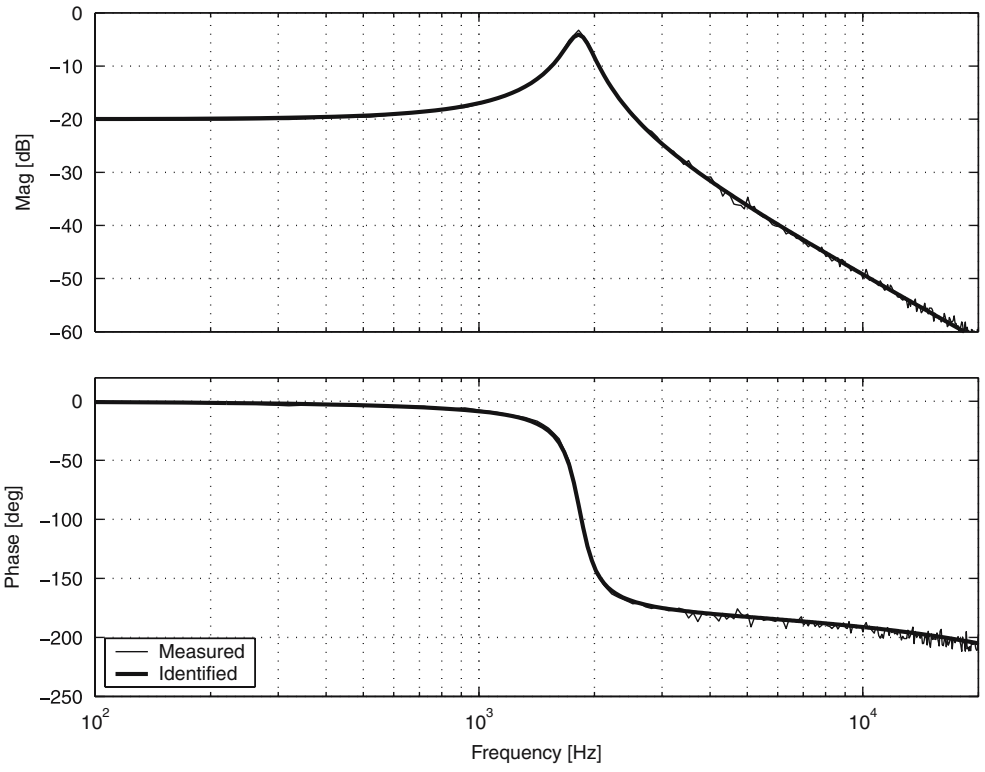

Fig. 5 Frequency response of the microactuator (Courtesy of Kenn Oldham)

as shown in Fig. 5. From the figure, we see that the MA has a single moderately damped mode at about 1.8 kHz, and there are no other significant modes up to 40 kHz. Thus it can be reasonably modelled as a single mass-spring-damper system with satisfying precision:

$$G_M(s) = \frac{A_m}{s^2 + 2\zeta_m \omega_m s + \omega_m^2}. \tag{2}$$

The parameters for G_M are $A_m = 0.2$ μm/V, $\zeta_m = 0.08$, and $\omega_m = 2\pi 1.85$ k rad/s.

2.4 The complete model

Combining the dynamics of the VCM-suspension assembly and the MA, and including the airflow disturbance, a double-input-double-output system can be obtained in state-space form:

$$\begin{bmatrix} \dot{x}_v \\ \dot{x}_n \\ \dot{x}_m \end{bmatrix} = \begin{bmatrix} A_v & 0 & 0 \\ 0 & A_n & 0 \\ 0 & 0 & A_m \end{bmatrix} \begin{bmatrix} x_v \\ x_n \\ x_m \end{bmatrix} + \begin{bmatrix} B_v & 0 \\ 0 & 0 \\ 0 & B_v \end{bmatrix} \begin{bmatrix} u_v \\ u_m \end{bmatrix} + \begin{bmatrix} B_{wv} \\ B_{wn} \\ 0 \end{bmatrix} w_a,$$

$$\begin{bmatrix} y_h \\ y_p \end{bmatrix} = \begin{bmatrix} C_h & 0 & C_m \\ C_p & C_n & 0 \end{bmatrix} \begin{bmatrix} x_v \\ x_n \\ x_m \end{bmatrix} + \begin{bmatrix} D_h & 0 \\ D_p & 0 \end{bmatrix} \begin{bmatrix} u_v \\ u_m \end{bmatrix}, \tag{3}$$

where x_v and x_n are the states of the off-track and non-off-track modes of the VCM-suspension assembly respectively, x_m is the state of the MA, u_v and u_m are the control inputs to the VCM and MA respectively, w_a denotes the airflow disturbance, and y_h and y_p are the head displacement and strain sensor output respectively.

3 Control design

The proposed control structure is illustrated in Fig. 6, where r denotes the track runout coming from various sources, such as the repeatable runout due to eccentricity of data tracks, disk flutter, spindle friction, etc. The overall controller consists of three loops: a feedback vibration damping loop closed around the VCM, a feedforward vibration compensation loop around the MA, and a dual-stage track-following servo loop. With

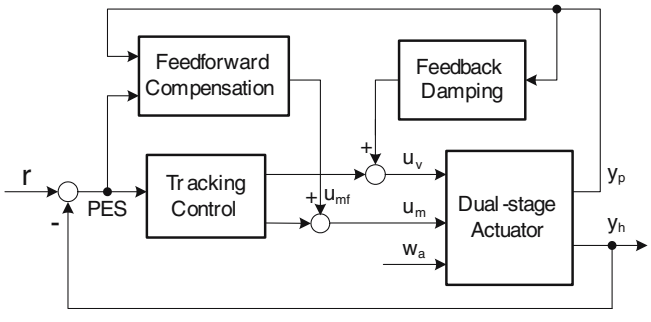

Fig. 6 Block diagram of the control system

a higher sampling rate of y_p, the vibration damping and compensation controllers will be implemented at a higher rate than the PES servo loop. In this study, the PES is assumed to be available at 25 kHz, while y_p and the RPES are sampled at 50 kHz. A computational delay, T_d, is also considered during design.

3.1 Vibration damping control design

The design of vibration damping control is formulated as a standard LQG problem. The effectiveness of this scheme has been experimentally verified in (Li et al. 2003). First, a discrete-time model with computational delay is obtained based on the augmented plant model (3), and can be written as

$$\begin{bmatrix} x_v(k+1) \\ x_n(k+1) \end{bmatrix} = \begin{bmatrix} \Phi_v & 0 \\ 0 & \Phi_n \end{bmatrix} \begin{bmatrix} x_v(k) \\ x_n(k) \end{bmatrix} + \begin{bmatrix} \Gamma_{sd} & \Gamma_d \\ 0 & 0 \end{bmatrix} \begin{bmatrix} u_v(k) \\ u_v(k-1) \end{bmatrix} + \begin{bmatrix} \Gamma_{wv} \\ \Gamma_{wn} \end{bmatrix} w_a(k),$$
$$y_p(k) = [C_p \quad C_n] \begin{bmatrix} x_v(k) \\ x_n(k) \end{bmatrix} + [0 \quad D_p] \begin{bmatrix} u_v(k) \\ u_v(k-1) \end{bmatrix} + v(k), \tag{4}$$

where $v(k)$ is the sensor measurement noise, and

$$\Phi_v = \mathrm{e}^{A_v T_s}, \quad \Gamma_{sd} = \int_{T_d}^{T} \mathrm{e}^{A\tau} B \mathrm{d}\tau,$$
$$\Phi_n = \mathrm{e}^{A_n T_s}, \quad \Gamma_d = \int_{0}^{T} \mathrm{e}^{A\tau} B \mathrm{d}\tau.$$

Γ_d reflects the effect of the computation delay. In this Kalman filter model, two design parameters can be tuned to set the bandwidth of the observer: the covariance matrix W of the airflow disturbance $w_a(k)$ and the covariance matrix V of the measurement noise $v(k)$.

By the separation principle of LQG design, the design of the feedback controller is also based on this model with some state rearrangements. Since at time instant k, $u_v(k-1)$ is already known, it can be put in the state vector leaving only the control input $u_v(k)$ to be determined:

$$\begin{bmatrix} x_v(k+1) \\ x_n(k+1) \\ u_v(k) \end{bmatrix} = \begin{bmatrix} \Phi_v & 0 & \Gamma_d \\ 0 & \Phi_n & 0 \\ 0 & 0 & 0 \end{bmatrix} \begin{bmatrix} x_v(k) \\ x_n(k) \\ u_v(k-1) \end{bmatrix} + \begin{bmatrix} \Gamma_{sd} \\ 0 \\ I \end{bmatrix} u_v(k),$$
$$y_h(k) = [C_h \quad 0 \quad D_h] \begin{bmatrix} x_v(k) \\ x_n(k) \\ u_v(k-1) \end{bmatrix}. \tag{5}$$

The cost function for this LQ design is

$$J = E\{y_h^2(k) + R u_v^2(k)\}, \tag{6}$$

where $E\{\cdot\}$ is the expectation operator, and the control action weight R can be tuned to achieve the desired system response.

Figure 7 shows the frequency response of the damped VCM-suspension assembly. Note that the two major resonance modes have been effectively damped, while there is little damping effect on the third mode due to its relatively small magnitude.

3.2 Feedforward compensation design

After the suspension resonance modes are damped by the VCM, the remaining vibration can be compensated by the MA. Because the MA is located at the suspension

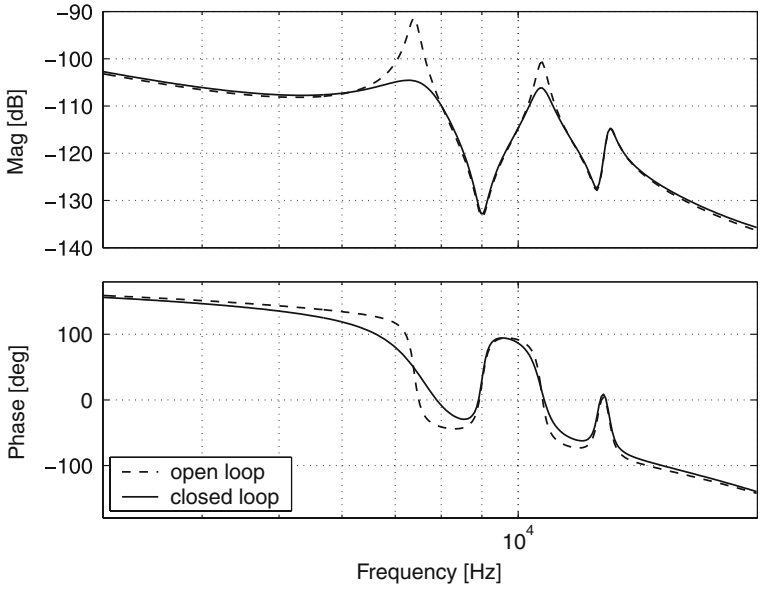

Fig. 7 Bode plot of the VCM-suspension assembly with/without damping control

tip as illustrated in Figs. 1 and 2, and its moving mass is much smaller than that of the VCM-suspension assembly, the MA has little effect on the suspension dynamics. In this case, feedforward control can be used to compensate the head motion due to suspension vibrations.

Define G_{wp} and G_{wh} as the transfer functions from w_a to y_p and y_h, respectively. Ideally, we want the two transfer functions to have the strongest correlation. However, since y_h and y_p represent the vibration effects at different locations, generally they are different and will probably have a dynamic relationship as shown in Eq. 3. We want the feedforward compensator, K_{MF}, to minimize the airflow-excited motion at the read/write head, i.e., to minimize

$$e_a = G_M K_{MF} G_{wp} w_a + G_{wh} w_a.$$

Intuitively, an expression for K_{MF} can be

$$K_{MF} = -G_M^{-1} \frac{G_{wh}}{G_{wp}}. \tag{7}$$

However, the expression in Eq. 7 may be noncausal, making it difficult to implement. Furthermore, the strain gauge factor, C_p, usually is sensitive to ambient temperature, and airflow disturbances are time-varying with different radial track positions. Thus, it is desirable to estimate the optimal filter K_{MF} online using some adaptation scheme.

In our approach, K_{MF} assumes a finite impulse response (FIR) filter for stability consideration:

$$K_{MF}(\theta, q^{-1}) = h_0 + h_1 q^{-1} + \cdots + h_n q^{-n}, \tag{8}$$

where θ is the filter coefficient vector $\theta = [h_0\ h_1\ \ldots\ h_n]^{\mathrm{T}}$ and n is the order of the FIR controller. The output of the MA by feedforward control can be expressed as

$$\begin{aligned} y_{MF}(K) &= G_M(q^{-1}) K_{MF}(q^{-1}) y_p(k) \\ &= K_{MF}(q^{-1}) G_M(q^{-1}) y_p(k) \\ &= K_{MF}(q^{-1}) x_f(k) \\ &= \theta^T \phi(k-1), \end{aligned} \tag{9}$$

where $x_f(k) = G_M(q^{-1}) y_p(k)$, $\phi(k) = [x_f(k) x_f(k-1) \cdots x_f(k-n)]^{\mathrm{T}}$. Since $x_f(k)$ is not measurable, it is estimated by passing $y_p(k)$ through the model of the MA, $\hat{G}_M$:

$$x_f(k) = \hat{G}_M(q^{-1}) y_p(k). \tag{10}$$

Some parameter adaptation algorithm can be used to adapt the coefficients of θ so as to minimize the mean square value of e_a, $E\{e_r^2(k)\}$. However, e_a is not directly available, and what we have access to is the position error signal, PES, which can be written as

$$e(k) = e_a(k) + e_r(k), \tag{11}$$

where e_r represents the component of the tracking error from all other disturbance sources except the airflow disturbances. It is roughly valid to assume that w_a and r are uncorrelated, then we have

$$E\{e^2(k)\} = E\{e_a^2(k)\} + E\{e_r^2(k)\}. \tag{12}$$

Thus, minimizing $E\{e_a^2(k)\}$ is equivalent to minimizing $E\{e^2(k)\}$, and we can use the PES as a corrupted error signal to perform the adaptation. With e_a corrupted by e_r, a little longer time is expected for the adaptation process to converge.

3.3 Track-following control design

Several methods have been used for designing dual-stage track-following servo systems, such as the master-slave method (Koganezawa et al. 1999), the PQ method (Schroeck and Messner 1999), μ-synthesis (Li and Horowitz 2002), and mixed H_2/H_∞ (Huang et al. 2004). In this paper, a straightforward method, called the sensitivity decoupling or the series compensation, is utilized (Mori et al. 1991; Li and Horowitz 2001b).

Figure 8 shows the block diagram of the dual-stage track-following controller using this design method. Decoupling of the whole sensitivity function is achieved by adding the RPES to the PES before feeding the PES to the VCM controller, K_V. Straightforward manipulation shows that the total closed-loop sensitivity transfer function can be expressed as a cascade of the sensitivity functions of the VCM and MA, i.e.,

$$S_T = S_V S_M. \tag{13}$$

With S_T decoupled, K_V and K_M can be designed sequentially using conventional design techniques, such as loop shaping or pole placement. After decoupling, it is clear that the VPES is the tracking error with the VCM actuator only; while the MA does further compensation to yield the final error, the PES. It is also noted that the motion of the MA relative to the

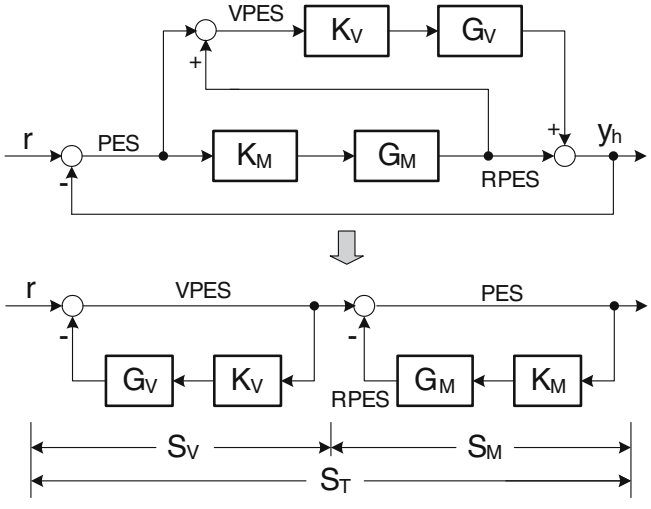

Fig. 8 Block diagram of the track-following controller

suspension should be available for decoupling. Capacitive sensing can be embedded in the MA structure to get the RPES. Frequency responses of three sensitivity transfer functions, S_V, S_M, and S_T, are shown in Fig. 9. In the design, the gain crossover frequency for the VCM loop is selected to be 700 Hz, and that for the MA loop is 3,500 Hz, while the total sensitivity function, S_T, achieves a bandwidth of 2.1 kHz.

4 Simulation results

4.1 Comparison between various configurations

First, the tracking performances, which is indicated by the RMS value of the PES, for various system configurations are compared. During simulation, the reference signal, r, is constructed from a combination of various sources, such as the repeatable track runout, disk flutter, low-frequency torque disturbances to the VCM, etc. Measurement noises and control input noises are also injected into the systems at proper locations. The results are shown in Fig. 10. In the figure, DS denotes the basic dual-stage track-following control without any specific vibration control; LQG denotes the vibration feedback damping control of the VCM-suspension assembly using y_p; FF denotes the adaptive feedforward vibration compensation of the MA using y_p. Different combinations mean different configurations of the control system. For example, DS_LQG_FF means both feedback damping of the VCM and feedforward compensation of the MA are used together with the dual-stage tracking control. From the figure, we can see that with only the DS control, there are two major resonance peaks resulting from the assembly butterfly mode M1 and suspension first torsion mode M2. With extended servo bandwidth and more attenuation in the low-frequency range, these resonance modes actually get amplified. Both feedback damping and feedforward compensation can attenuate these peaks. But in DS_LQG, some regions between the peaks get amplified due to the tradeoff effect in these regions; while in DS_FF, a net reduction is achieved across the frequency range. Also note that in DS_FF, two small peaks show up in between 2-4 kHz. They result from the non-off-track modes entering the strain sensor output signal. Increasing the order of the feedforward compensator can suppress these peaks and improve the feedforward compensation effect. The combination of LQG and FF yields the best tracking performance of from 7.55 nm for DS to 5.82 nm for DS_LQG_FF, achieving an improvement of about 23%.

4.2 Normal sensing versus improved sensing

The system performance is also affected by the sensing quality of the strain gauge sensor. Intuitively, we want to have the largest correlation between the strain sensor output, y_p, and the actual head position, y_h. This implies that the sensor should only pick up those off-track modes and reject those non-off-track modes. This property may be achieved by optimizing the sensor design in its location, orientation, and shape (Huang et al 1999; Oldham et al. 2003). When the sensor only picks up those off-track modes, a lower order damping controller can be designed for fast implementation, and better performance can be achieved with feedforward compensation since the signal is less contaminated.

The performance comparison between normal sensing and improved sensing is shown in Fig. 11. Here, normal sensing means sensing with non-off-track modes entering the signal, while improved sensing means

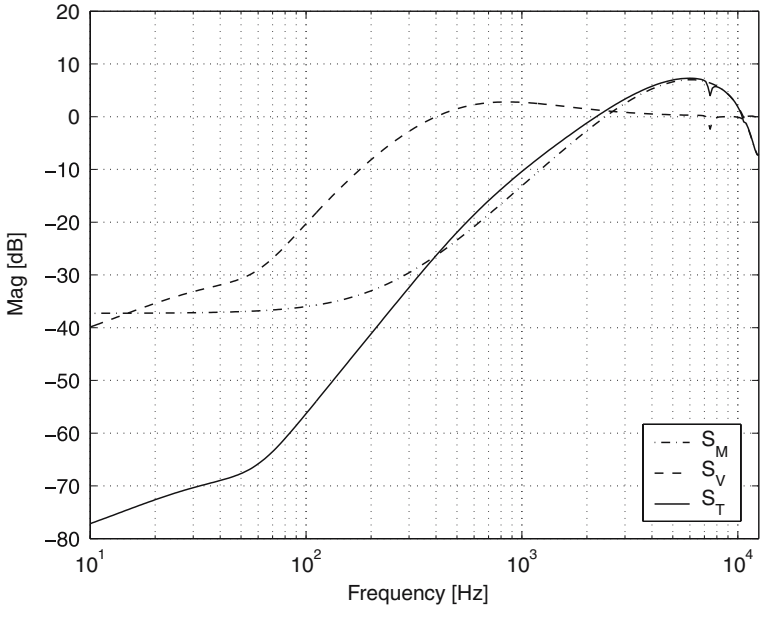

Fig. 9 Sensitivity frequency responses of S_V, S_M, and S_T

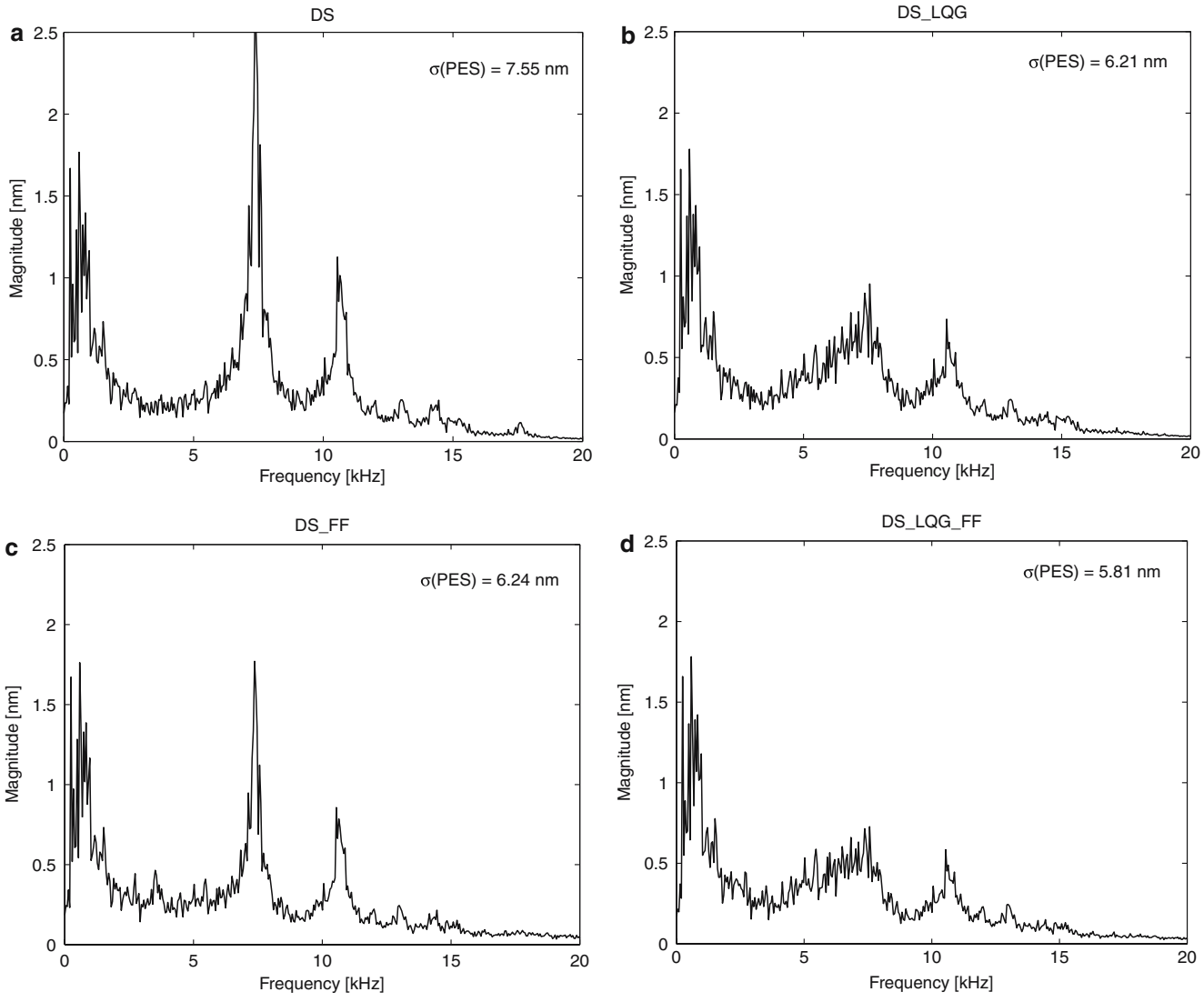

Fig. 10 RMS values of the PES for various system configurations: **a** Only with track-following control. **b** Track-following plus feedback vibration damping. **c** Track-following plus feedforward vibration compensation, **d** Track-following with feedback vibration damping and feedforward compensation

sensing without non-off-track components. It is seen that with improved sensing, the vibration peaks can be further suppressed and the RMS value of the PES is decreased from 5.82 nm for normal sensing to 5.60 nm for improved sensing, achieving a further improvement of 4%.

Figure 12 shows the RMS value of the PES for various configurations. Feedforward compensation is a little more sensitive to the sensing quality than feedback damping. The combination of feedback damping and feedforward compensation always yield the best performance.

5 TMR sources analysis with projection to 500k TPI

In the disk drive industry, track following servos are traditionally designed in the frequency domain before a drive is built. Time domain performance characteristics are not evaluated until a prototype drive is built and servo code is implemented. With rapid increase in TPI, one by one generation of disk drives is being developed and batch fabricated. Prediction of future products performance is desired and often crucial. From prediction, one may roughly know what performance can be achieved with those technologies and improvements to be applied to the new product, and what are the main remaining problems or obstacles to further performance improvement. With the targeted 3σ PES of 5 nm, there is still a long way to go before approaching it. Much work has already been done on TMR sources identification, characterization and performance projection. Based on those results available at present, and the design methodology and simulation results for the dual-stage servo system presented in this paper, a more realistic performance projection can be performed.

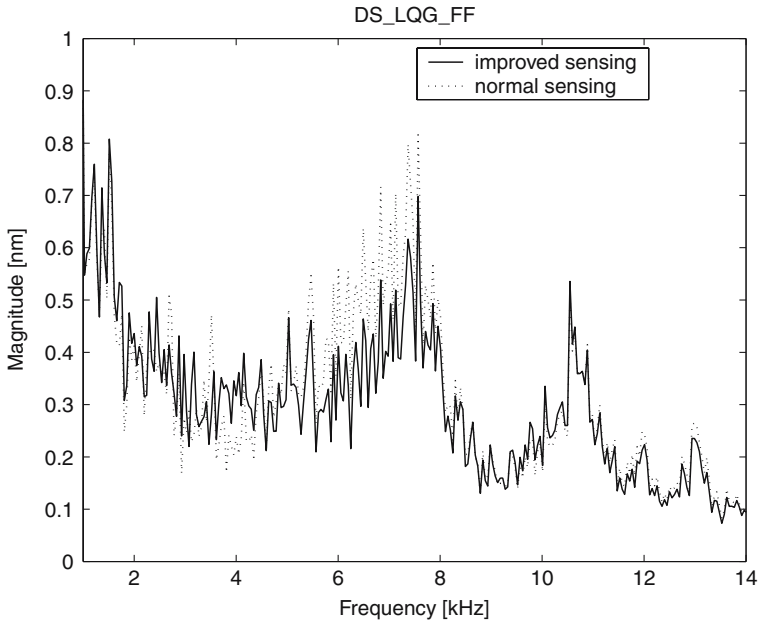

Fig. 11 Performance comparison between normal/improved sensing

First, TMR sources are decomposed and characterized in detail before doing performance projection. In general, TMR sources are classified into two categories: repeatable runout (RRO) and non-repeatable runout (NRRO). RRO is synchronous with the spindle revolution and is caused by both imbalance in the spindle and imperfections in the servo-written track circles, while NRRO is caused by various disturbance sources such as airflow turbulence, disturbances due to ball bearing defects, spindle and disk resonance modes, disturbance from adjacent disks, and external shock and vibration. In this study, TMR sources are classified into 6 items: (1) RRO; (2) disk runout, including disturbances from spindle and disk motion; (3) VCM torque disturbances, including low-frequency (<2 kHz) disturbances from printed flexible cable, spindle friction, spindle and disk resonance modes, and current amplifier nonlinearity; (4) Airflow-excited suspension vibrations, which lie in the high-frequency range (>2 kHz); (5) MA torque disturbances, which mainly result from airflow disturbances; (6) PES measurement noise, which is related to the PES demodulation noise and quantization noise. It should be noted that, disturbance from adjacent disks and external shock and vibration are not included in the analysis. This is mainly because the two disturbance sources are difficult to characterize and project. The two disturbances depend on the specific hard disk configuration and actual working conditions. As far as the authors are aware, till now there is no research result on the two disturbance sources that are reported in the literature.

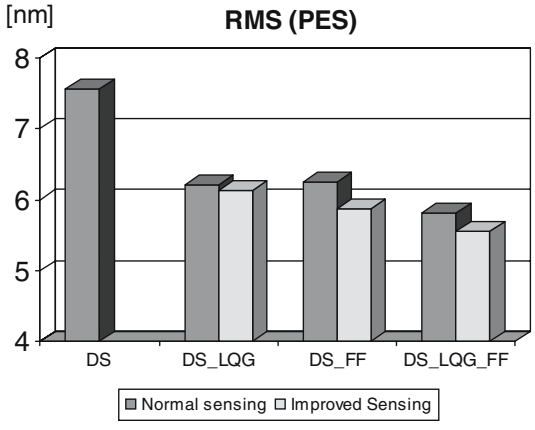

Fig. 12 Performance comparison between various configurations

Performance projection is carried out based on the following assumptions:

1. Compared with ball bearing, a fluid bearing spindle will reduce spindle NRRO by a factor of 4 (Guo and Chen 2001).
2. Disk flutter, arm torque disturbances and suspension vibrations decrease with $D^{1.4}$ (Srikrishna and Kasetty 2000; Guo and Chen 2001; Gross 2003), and airflow disturbances decrease with D^2, where D is the disk diameter.
3. Disk flutter is reduced by a factor of three due to the use of new disk substrate materials and the increase in its thickness (Srikrishna and Kasetty 2000; Guo and Chen 2001).
4. By using a redesigned, stiffer suspension with higher vibration modes, the level of airflow disturbances is reduced by a factor of 2.
5. The PES measurement noise scales with the track pitch (fixed percentage of the track pitch) (Ehrlich and Curran 1999; Ehrlich 1999).

The performance projection results are summarized in Table 1. These values are calculated from the time domain disturbance sequences used in the simulation. The first scaling results from the combination of disk

Table 1 TMR source decomposition with projection to 500k TPI

Closed-loop TMR components (1σ value) Unit: (nm)	100k TPI 7,200 RPM 3.5″ disk	Scaling	500k TPI 7,200 RPM 3.5″ disk	Scaling	500k TPI 7,200 RPM 2.5″ disk	Open-loop TMR components
	Sampling rate = 25/50 kHz, Servo bandwidth = 2.1 kHz					
RRO (written-in runout)	3.578	1/4	0.895	1	0.895	141.12
Disk runout	1.867	1/4	0.467	0.62	0.290	13.96
VCM torque disturbance	0.385	1	0.385	0.62	0.239	128.84
Suspension vibration	3.711	1	3.711	0.62	2.301	4.10
MA torque disturbance	0.820	1	0.820	1	0.820	1.00
Measurement noise	1.209	1/5	0.242	1	0.242	1.00
Total RMS value	5.60		3.96		2.64	195.43
	Sampling rate = 40/80 kHz, Servo bandwidth = 3 kHz					
RRO (written-in runout)	2.050	1/4	0.513	1	0.513	
Disk runout	0.649	1/4	0.162	0.62	0.100	
VCM torque disturbance	0.151	1	0.151	0.62	0.094	
Suspension vibration	3.002	1	3.002	0.62	1.861	
MA torque disturbance	0.465	1	0.465	1	0.465	
Measurement noise	1.029	1/5	0.206	1	0.206	
Total RMS value	3.97		3.10		2.00	

platter redesign, the use of fluid bearing, and the increase in TPI. Measurement noise reduction solely results from the increase in TPI. The second scaling is due to the reduction in disk size, which will reduce airflow speed and turbulence level.

Another effective way of improving performance is to increase the sampling rate of the PES. This sampling rate cannot be increased arbitrarily in practice because it is determined by the hardware configuration: how much fraction of the disk space is allocated for embedded track position information, or equivalently, for servo sectors. If this sampling rate could be increased, then the closed-loop servo bandwidth can be increased accordingly and high-frequency disturbances will be less amplified. From the table we see that, when the dual sampling rates are increased from 25/50 kHz to 40/80 kHz, the performance is improved by about 30%. Under a typical disk drive configuration, the servo sectors occupy about 5% of the total disk space. This means that doubling the number of servo sectors implies 5% more space required for servo sectors. During the continuous increase in track density, it seems feasible to allocate a little more disk space for position information storage.

The final point to be addressed here is that with all those scalings and improvements, airflow-excited suspension structural vibrations have become the most important contributor to the closed-loop TMR. This is partially due to the fact that structural vibrations are largely in the high-frequency range and are difficult to be suppressed by the PES servo loop. Another reason is that little information on vibration suppression by mechanical design can be collected from the literature, because this is generally kept as a technique secret by disk manufacturers. But from these projection results, we can still say that with substantial reduction in the airflow-excited structural vibrations, it is possible to approach the targeted track density of 500k TPI, or 3σ TMR of 5 nm.

6 Conclusion

In this paper, a track-following control design with active vibration damping and compensation was proposed for a VCM-MEMS MA dual-stage servo system. Airflow-excited suspension vibrations were modelled and controlled with the aid of a vibration signal from a strain sensor on the suspension. Vibration control is implemented by a feedback damping loop around the VCM actuator and a feedforward compensation loop around the MA. The feedback damping loop is designed using the LQG technique, while the feedforward compensation loop is based on an adaptive control scheme. Both of the two controllers are updated at a higher rate than that of the PES servo loop for better control effect. Simulation results show the effectiveness of the proposed control scheme in attenuating airflow-excited structural vibrations and enhancing the closed-loop performance of the servo system.

Simulation study also shows the potential improvement with improved sensing, in which the vibration sensor only senses those TMR-related off-track vibration modes, while be insensitive to those non-off-track modes. Besides, with improved sensing, the LQG control design will also be simplified since those non-off-track modes do not have to be modelled and therefore less computation time is needed. Improved sensing is also helpful for improving feedforward compensation effect. Optimization in sensor location, orientation and shape has become an important topic for vibration control.

Performance projection to 500k TPI was carried out, from which we see what are possible technique innovations and configurations that can help further decrease the TMR value. With substantial reduction in the airflow-excited structural vibrations, it is possible to achieve the targeted track density of 500k TPI, or equivalently, 3σ TMR of 5 nm.

Acknowledgements Research supported by the Information Storage Industry Consortium (INSIC) and the Computer Mechanics Laboratory (CML) of U.C. Berkeley

References

Bode HW (1945) Network analysis and feedback amplifier design. Van Nostrand, New York

Ehrlich R (1999) High track density servos—understanding sources of TMR. 1999 NSIC tracking team meeting

Ehrlich R, Curran D (1999) Major HDD TMR sources and projected scaling with TPI. IEEE T Magn 35(2):885–891

Gross HM (2003) Off-track vibrations of the read-write heads in HDDs. PhD thesis. Department of Mechanical Engineering, University of California, Berkeley

Guo L, Chen YJD (2001) Disk flutter and its impact on HDD servo performance. IEEE T Magn 37(2):866–870

Huang Y, Banther M, Mathur PD, Messner W (1999) Design and analysis of a high bandwidth disk drive servo system using an instrumeted suspension. IEEE/ASME T Mech 4(2):196–206

Huang FY, Semba T, Imaino W, Lee F(2001) Active damping in HDD actuator. IEEE T Magn 37(2):847–849

Huang X, Nagamune R, Horowitz R, Li Y (2004) Design and analysis of a dual-stage disk drive servo system using an instrumented suspension. In: Proc Am Control Conf 4:535–540

Koganezawa S, Uematsu Y, Yamada T (1999) Dual-stage actuator system for magnetic disk drives using a shear mode piezoelectric microactuator. IEEE T Magn 35(2):988–992

Li Y, Horowitz R (2001a) Active suspension vibration control with dual-stage actuators in hard disk drives. In: Proc Am Control Conf 4:2786–2791

Li Y, Horowitz R (2001b) Mechatronics of electrostatic microactuators for computer disk drive dual-stage servo systems. IEEE/ASME T Mech 6(2):111–121

Li Y, Horowitz R (2002) Design and testing of track-following controllers for dual-stage servo systems with PZT actuated suspensions. Microsyst Technol 8:194–205

Li Y, Marcassa F, Horowitz R, Oboe R, Evans R (2003) Track-following control with active vibration damping of a PZT-actuated suspension dual-stage servo system. In: Proc Am Control Conf 3:2553–2559

Mori K, Munemoto T, Otsuki H, Yamaguchi Y, Akagi K (1991) A dual-stage magnetic disk drive actuator using a piezoelectric device for a high track density. IEEE T Magn 27(6):5298–5300

Oboe R (2000) Use of low-cost MEMS accelerometers for vibration compensation in hard disk drives. In: Proc of the 6th international workshop on advanced motion control, pp 485–489

Oldham K, Kon S, Horowitz R (2003) Fabricatin and optimal strain sensor placement in an instrumented disk drive suspension for vibration suppression. Technical report 10. CML Blue Report, Department of Mechanical Engineering, University of California, Berkeley

Pannu S, Horowitz R (1999) Increased disturbance rejection for hard disk drives using accelerometers. J Inf Stor Proc Syst 1:95–103

Schroeck SJ, Messner WC (1999) On controller design for linear time-invariant dual-input single-output systems. In: Proc Am Control Conf 6:4122–4126

Seagate (2003) Seagate sets the areal density storage record. http://www.seagate.com/newsinfo/technology/d4g.html

Srikrishna P, Kasetty K (2000) Predicting TMR from disk vibration of alternate substrate materials. IEEE T Magn 36(1):847–849